Computational Fluid Dynamic (CFD) Simulation Thermal Performance and Hydrodynamic Erosion in Circulation Fluidized Bed (CFB) Boiler at PLTU West Kalimantan Title of Manuscript

Eflita Yohana[1,*], Mohamad Said Kartono Tony Suryo[1], Ahmad Musawwir Azhim[1], Muhammad Salman Al Farisi[1], Indah Hartati[2], Mohammad Farkhan Hekmatyar Dwinanda[3], Kwang-Hwan Choi[4]

[1] Department of Mechanical Engineering, Diponegoro University, Jl. Prof. Sudharto, SH, Semarang 50275, Indonesia
[2] Department of Chemical Engineering, Wahid Hasyim University, Semarang, Indonesia
[3] Department Energy Conservation & Loss Control, Engineering Development, PT. Kilang Pertamina International, Balikpapan, Indonesia
[4] Department of Refrigeration and Air Conditioning Engineering, Pukyong National University, Busan, South Korea

ARTICLE INFO

ABSTRACT

Computational Fluid Dynamics (CFD) has been widely used to study Circulation Fluidized Bed (CFB) combustion processes. Analysis of mixed fuel between coal and biomass from PKS (palm kernel shell) in the combustion process that occurs in the boiler at West Kalimantan power plant is carried out by mixing the addition of PKS fuel by 20%, 40%, 60%, and 80%. The simulation uses model set-up data, material properties, and boundary conditions according to PJB (Pembangkitan Jawa Bali) Ketapang's experimental data. Then an analysis was carried out with a fluid flow velocity of 3.2 kg/s and particle sizes of 150 μm, 300 μm, 400 μm, and 500 μm on the erosion rate that occurs on the furnace walls due to sand particles present in the combustion process material at the Steam Power Plant (PLTU). Based on the simulation results of mixing fuel between coal and PKS variations of 20% - 80%, the temperature decreased from 1180℃ – 920.03℃ due to differences in fuel heat. Whereas the erosion rate in the simulation has increased from 0.000189 kg/s – 0.001886 kg/s due to differences in the size of the sand particles and the velocity of the mass flow rate of the particles.

1. Introduction

Indonesia has proven reserves of coal that can be produced for up to 2100 or 80 years, as said by the Director General of Mineral and Coal. Therefore, the coal production quota was limited to around 500 tons/year. Indonesia's real step in limiting coal fuel is by building a renewable energy (EBT) project. In this context, the government will also keep supporting the growth of a number of renewable energy (EBT)-based power generation projects, including hydropower (PLTA) and biomass (PLTBM). The contribution of EBT has barely reached 12.52%, according to the National Energy Mix. In the 2019-2028 Electricity Provision General Plan (RUPTL), the National Energy Mix target for EBT

power generation increases to 23% in 2025 [1]. Global climate change is now taking place, which affects natural disasters around the planet. Indonesia is dedicated to helping find solutions to global climate change, according to the United Nations Framework Convention on Climate Change (UNFCCC). To address the problem of global climate change various solutions are offered. Reduced emissions of greenhouse gases (GHGs), which are brought on by burning fossil fuels like coal and oil, as well as deforestation and forest fires, are one way to combat global warming. [1].

As a source of energy that contains carbon, biomass can be a significant contributor to the use of renewable energy. The potential for biomass in PLTBM is to use Palm Kernel Shells (PKS) derived from processing palm oil shells. Indonesia produces 9.2 million tons of palm kernel shells per year. The duties on exports did, however, increase at this time. As a result, the nation has to use palm shells more frequently. In order to diversify its fuel supply and promote mitigation of the effects of greenhouse gas reduction, the Ketapang PLTU has introduced and enhanced the usage of PKS (palm kernel shell) biomass. The use of PKS (palm kernel shell) is expected not to exceed the temperature protocol at the PLTU Boiler. The temperature value does not exceed 950°C before entering the Boiler.

Fluidized-bed combustion is a development tool for conventional stokers and pulverized-fuel combustion. Generally used for furnace applications, such as in the process of producing hot gas for drying. In reducing the gas drying temperature excess air is added or flue gas recirculation is carried out [2]. The working mechanism of Fluidized Bed Combustion is that primary air is ejected by a blower from under the combustion chamber, then secondary air carries solid fuel into the side of the combustion chamber, while the burner is installed on the side adjacent to the primary air [3]. Furthermore, solid fuel is burned by the burner. The disadvantage of a solids fuel combustion system is that it has a low density, so not all of it is burned by the burner. Whereas solid fuels have unequal densities, small densities will fly out of the combustion chamber and large densities will fall, where it forms an agglomeration, resulting in incomplete combustion [4, 5].

Features in Fluidized Bed Combustion (FBC) is the occurrence of direct contact of particles with intensive heat and mass changes [6]. The uniform temperature in Fluidized Bed Combustion has a high heat capacity which will burn lower quality fuel, in which case regulation of bed temperature by fuel supply, air, and heat extraction will be more effective [7, 8].

In Fluidized-Bed Combustion, The most important parameter in FBC or packing is the velocity of the fluid passing through the top of the particle bed barrier [9]. Then the two beds are mounted on a vessel that will channel the fluid into the bed which is called a distributor. In addition, there is also a compressor as a tool for fluidization in the fuel feeder. There are many studies regarding numerical analysis of fluidized beds using CFD, including Kumar *et al.,* [10], Suksuwan *et al.,* [11], Liu *et al.,* [12]. In this research, the author uses CFD (Computational Fluid Dynamics) to analyse fluid flow in Fluidized Bed Combustion (FBC).

2. Methodology
2.1 CFD (Computational Fluid Dynamic)

CFD (Computational Fluid Dynamics) is a numerical technique for solving regulatory equations in a given fluid flow which can be described using Navier's Stoke equation. The CFD code is composed of numerical algorithms that can solve fluid flow problems [13]. A CFD code consists of three main elements, namely the pre-processor, solver, and post-processor. Continuity for a compressible fluid in steady-state flow in the notation can be seen in Eq. (1) below:

$$\frac{\partial \rho}{\partial t} + d_{iv}(\rho u) = 0 \tag{1}$$

For incompressible flow, the density ρ is constant, and Eq. (1) becomes

$$D_{iv}(u) = 0 \tag{2}$$

Then the momentum equation is as follows.

$$\frac{\partial(\rho u_i)}{\partial t} + \frac{\partial(\rho u_i u_j)}{\partial x_j} = -\frac{\partial p}{\partial x_i} + \frac{\partial}{\partial x_j}\mu\left(\frac{\partial u_i}{\partial x_j} + \frac{\partial u_j}{\partial x_j} - \frac{2}{3}\frac{\partial u_k}{\partial x_k}\delta_{ij}\right) + \rho g_i + F_i \tag{3}$$

The k- ε turbulent model consists of turbulent kinetic energy and energy rate of dissipation

$$\frac{\partial}{\partial t}(\rho k) + \frac{\partial}{\partial x_i}(\rho k u_i) = \frac{\partial}{\partial x_j}\left[\left(\mu + \frac{\mu_t}{\sigma_t}\right)\frac{\partial_k}{\partial_k}\right] + G_k + G_b - \rho\varepsilon - Y_m + S_k \tag{4}$$

$$\frac{\partial}{\partial t}(\rho\varepsilon) + \frac{\partial}{\partial x_i}(\rho\varepsilon u_i) = \frac{\partial}{\partial x_j}\left[\left(\mu + \frac{\mu_t}{\sigma_t}\right)\frac{\partial_t}{\partial_{xj}}\right] + C_{1\epsilon}\frac{\epsilon}{k}(G_k - C_{3\epsilon}G_b) - C_{2\epsilon}\rho\frac{\epsilon^2}{k} + S_\in \tag{5}$$

The completion of the form of the energy equation, can be seen in Eq. (6) [14].

$$\frac{\partial(\rho\epsilon)}{\partial t} + \frac{\partial}{\partial_{xj}}(u_i(\rho E + p)) = \frac{\partial}{\partial_{xj}}\left[\left(K_{eff}\frac{\mu_t}{\sigma_\epsilon}\right) - \Sigma_j h_i J_j + u_i(\tau_{ij})\right] + S_h \tag{6}$$

The turbulence equation uses the standard k-ε model according to the simulation setup. This modeling is used even though it is still simple, allowing for two equations, namely turbulent velocity and length scale, the length scale is determined independently. This model has stability, is economical in terms of computation, and sufficient accuracy makes this model often used in fluid and heat transfer simulations. The standard k-ε formula can be seen in Eq. (7) and (8).

$$\frac{\partial}{\partial t}(pk) + \frac{\partial}{\partial x_i}(pk u_i) = \frac{\partial}{\partial x_j}\left[\left(\mu + \frac{u_t}{\sigma_k}\right)\frac{\partial_k}{\partial_{xj}}\right] + G_k + G_b - \rho\epsilon - Y_m + S_k \tag{7}$$

$$\frac{\partial}{\partial t}(p\epsilon) + \frac{\partial}{\partial x_i}(p\varepsilon u_i) = \frac{\partial}{\partial x_j}\left[\left(\mu + \frac{u_t}{\sigma_\epsilon}\right)\frac{\partial_\varepsilon}{\partial_{xj}}\right] + C_{1\in}\frac{\in}{k} + (G_k - C_{3\varepsilon}G_b) - C_{2\epsilon}\rho\frac{\varepsilon^2}{k} + S_k \tag{8}$$

2.2 Geometry and Mesh

This research is based on previous experiments at the Steam Power Plant (PLTU) in West Kalimantan. The boiler has a capacity of 2 × 10 MW with coal fuel and has dimensions of length 21.8 m, width 16.7 m, and height 41.0 m as shown in Figure 1. The boiler consists of two parts, namely a combustion chamber and two cyclone separators with four inlet channels. Which are two primary fuel-air passages for fluidization at the bottom of the combustion chamber and two secondary fuel-air passages to distribute sufficient air for coal particle combustion. The meshing results of the furnace are shown in Figure 2.
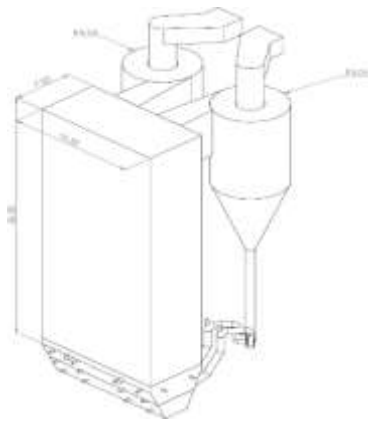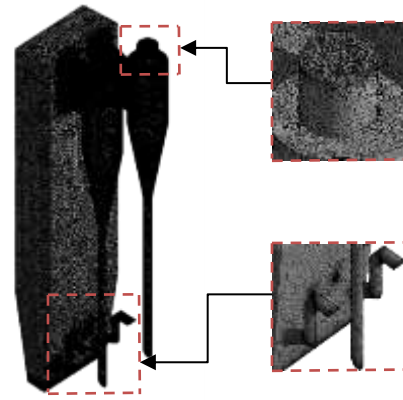
Fig. 1. 3D furnace geometry

Fig. 2. Results of meshing furnace

The meshing created refers to the rule of thumb which is generally used to assess mesh quality based on skewness. The mesh process that has been carried out has an average skewness value of 0.22827 and meets fairly good quality. Skewness is used to show how slanted a mesh is. The more angular an element is, the better the transfer of data from one element to another, so that when the shape of an element is skewed it will require quite a lot of corrections during the computation process which reduces the quality of calculations and slows down the computation process.

2.3 Grid Independent

In the meshing process, the Cut Cell method is used which has the advantage of more regular domain cells compared to Tetra-Mesh and Hexahedral. Fulfillment of grid quality values in meshing is carried out using the determinant method which aims to ensure that the simulation runs without burdening the computer and obtains an optimal mesh, so it is necessary to carry out an independent grid test. The number of element levels in testing ranging from 1,000,000 to 4,500,000 is used to get the best grid value results. Figure 3 shows a graphic comparison of the number of elements to temperature. Based on each variation, the number of elements shows an increase as the number of elements increases and begins to stabilize at element variations of 3,500,000 – 4,500,000. Based on the graphical results to obtain the optimal mesh and does not depend on the number and type of mesh, the number of 4,000,000 grid elements is selected to be used in the simulation process.
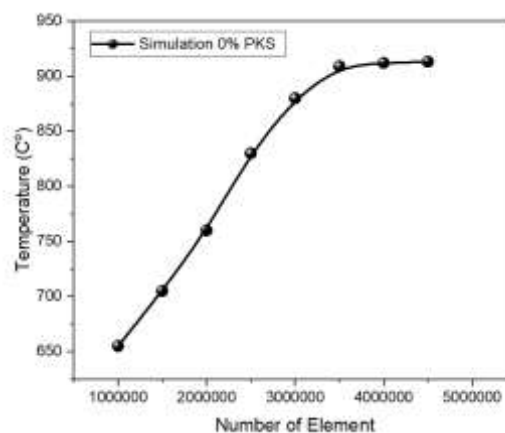

Fig. 3. Grid independent

From the graph above, with a number of elements of 4,000,000, the temperature value is 912 ℃. Experiments carried out by the West Kalimantan PLTU produced Furnace Bed Temperature and Furnace Exit Gas Temperature values of 966.85 ℃ and 906.75 ℃.

2.4 Combustion Model

The combustion model is analyzed numerically to determine the combustion process that occurs in the boiler. Based on data from the West Kalimantan PLTU, this simulation was carried out at full load using the *K-ε* Standard turbulence model. Combustion reactions consist of devolatilization processes, gas oxidation, char oxidation, and gasification. Combustion reactions calculated based on the Ultimate and Proximate analysis of coal fuel are shown in Table 1.

Table 1
Coal Analysis AR Basis (%)

Proximate		Ultimate	
Volatile	0.27	C	0.65258
Fixed carbon	0.28998	H	0.10409
Ash	0.03989	O	0.22683
Moisture	0.36383	N	0.01297
		S	0.0022
GCV (MJ/kg)		19049.75	

The amount of coal needed is calculated based on the boiler load of 2 × 10 MW and the heating value (19049.75), while the oxidizer in the form of air is given to the combustion process, which is calculated by taking into account the consumption of coal and the excess air needed.

2.5 Erosion Model
2.5.1 Finnie's erosion model

Based on several assumptions, Finnie proposed two equations to estimate the volume of material lost by a single abrasive grain for low and high-impact angles, which can be written in Eq. (9) and (10) below:

$$\varepsilon_{VP} = \frac{m_p V_p^2}{\rho \Psi k}\left(\sin(2\alpha) - \frac{6}{K}\sin^2(\alpha)\right) \text{ for } \tan\alpha \leq \frac{K}{6} \tag{9}$$

$$\varepsilon_{VP} = \frac{m_p V_p^2}{\rho \Psi k}\left(\frac{k\cos^2\alpha}{6}\right) \text{ for } \tan\alpha \geq \frac{K}{6} \tag{10}$$

where ε_{VP} is the volume of displaced surface material, m_p is the mass of the particle, V_p is the particle velocity, p is the plastic flow stress constant, α is the particle impact angle, K is the ratio of the vertical force component on the particle surface to the horizontal force component. Ψ is the ratio of contact depth I to Y_t has a constant value. Finnie uses a value of 2 for this parameter. The first equation holds for low impact angles which correspond to the circumstances in which the particles leave the surface while cutting. The second equation applies to high impact angles in circumstances where the horizontal motion of the particle tip stops when cutting [15].

2.5.2 McLaury's erosion model

McLaury proposed a model to predict the erosion rate of particles with water as a carrier fluid. This model was developed to simulate the erosion rate in liquid-solid (slurry) flows. The McLaury model is written in Eq. (11) as follows:

$$E = AV^2 f(y)$$
$$A = F\, Bh^k \tag{11}$$

with the equation:

$$f(y) = by^2 + cy \quad for\ y \leq y_{\lim}$$
$$f(y) = x\cos^2 y \sin(wy) + y \sin^2(y) + z \quad for\ y > y_{\lim} \tag{12}$$

The values of the constants b, c, w, x and y in Eq. (12) above are determined experimentally. The z value is determined in such a way that the two angle function equations above are close together at $y = y_{\lim}$, where $y_{\lim}$ is the transition angle [16].

2.5.3 Oka's model erosion

The Oka erosion model was developed based on tests carried out on several types of target materials, such as pure iron, aluminum, carbon steel and stainless steel. The erosion rate due to the collision of the particles with the target material at the impact angle α is expressed according to Eq. (13) below:

$$E(\alpha) = g(\alpha)E_{90} \tag{13}$$

E_{90} is the erosion rate at an impact angle of 90°, and $g(\alpha)$ is a normalized impact angle function, expressed by two trigonometric functions and the initial material hardness number Hv (in GPa), according to Eq. (14) below:

$$g(\alpha) = (\sin\alpha)^{n1}(1 + Hv(1 - \sin\alpha))^{n2} \tag{14}$$

$n1$ and $n2$ are exponents determined by material hardness and other impact conditions such as particle properties, including particle shape. $g(\alpha)$ is determined based on Graphical Representation $g(\alpha)$ 13. The first term of Eq. (13) describes the repeated plastic deformation or brittle characteristics and with the vertical component of the particle impact energy if $n1$ = 2. The second term represents the shearing phenomenon, where erosion is relative and more effectively occur at lower impact angles [17]. E_{90} is expressed in Eq. (15) below:

$$E_{90} = K(Hv)^{k1}(v)^{k2}(D)^{k3} \tag{15}$$

where $k1$, $k2$ and $k3$ are the exponential factors that are influenced by other parameters. K is an arbitrary unit indicating particle properties such as shape and degree of hardness, which have different values for different types of particles. Ansys Fluent has entered these empirical constant values into each erosion model, so users only enter fluid, particle and target material parameters.

2.6 Boundary Condition

To get results that are close to and by the Fluidized Bed Boiler circulation in the West Kalimantan PLTU, it is necessary to enter the boundary condition values that are by the experimental data that has been carried out by the company. Based on data from the West Kalimantan PLTU, the condition of this simulation system occurs in a steady state. The boundary conditions can be seen in Table 2.

Table 2
Boundary condition

Properties	Type	Phase	Input Value	Source
Primary Air	Mass flow inlet	Air	ṁ = 10.5 kg/s	PLTU West Kalimantan
		Sand	T = 126 °C	
			Pgage = 10.1 kPa	
			ṁ = 3.2 kg/s	
Secondary Air	Mass flow air inlet	Air	ṁ = 7.4 kg/s	PLTU West Kalimantan
		Sand	T = 140 °C	
			Pgage = 2.3 kPa	
Coal Inlet	Mass flow coal inlet	Coal	ṁ = 10.5 kg/s	PLTU West Kalimantan
		Air	T = 126 °C	
			ṁ = 1 kg/s	
Pressure Inlet	Pressure inlet	Mixture	Pgage = 36 kPa	PLTU West Kalimantan

2.7 Variation of Coal Mixing Data and PKS (Palm Kernel Shell)

In this research simulation, the variation of the data is carried out on the value of the coal calculator in each variation of the simulation. The coal calculator value refers to the Proximate & Ultimate Analysis value of coal and Palm Kernel Shell (PKS). The percentage of mixing of coal and PKS is carried out at variations of 20%, 40%, 60%, and 80%. Apart from the Proximate & Ultimate Analysis data properties, everything still follows the data from the West Kalimantan PLTU. The Proximate & Ultimate variation values in the simulations carried out can be seen in Table 3.

Table 3
Proximate and ultimate simulation value variations

Proximate Analysis	20% PKS	40% PKS	60% PKS	80% PKS
Tm	0.315006	0.2663	0.266298	0.168766
Ash	0.33392	0.02689	0.026894	0.013898
Vol	0.352	0.434	0.432	0.598
Fc	0.26798	0.24599	0.24597	0.201996
Ultimate Analysis	20% PKS	40% PKS	60% PKS	80% PKS
C	0.61806	0.58355	0.583548	0.514516
H	0.09427	0.08445	0.084454	0.064818
N	0.01074	0.0085	0.008502	0.004034
O	0.24746	0.2681	0.268098	0.309366
S	0.01176	0.02132	0.02132	0.04044
Total GCV	17538.7	17840.9	18142.4	18434.2

2.8 Post Processing

Retrieval of contour data is carried out on several planes based on their height and axis. The location of the planes can be seen in Figure 4. Where planes A to plane F show the ZX position for measuring the height of the furnace, while the Furnace Bet Temperature (FBT) and Furnace Exit Gas

Temperature (FEGT) are the locations for taking the contours by experiments conducted by PLTU West Kalimantan.
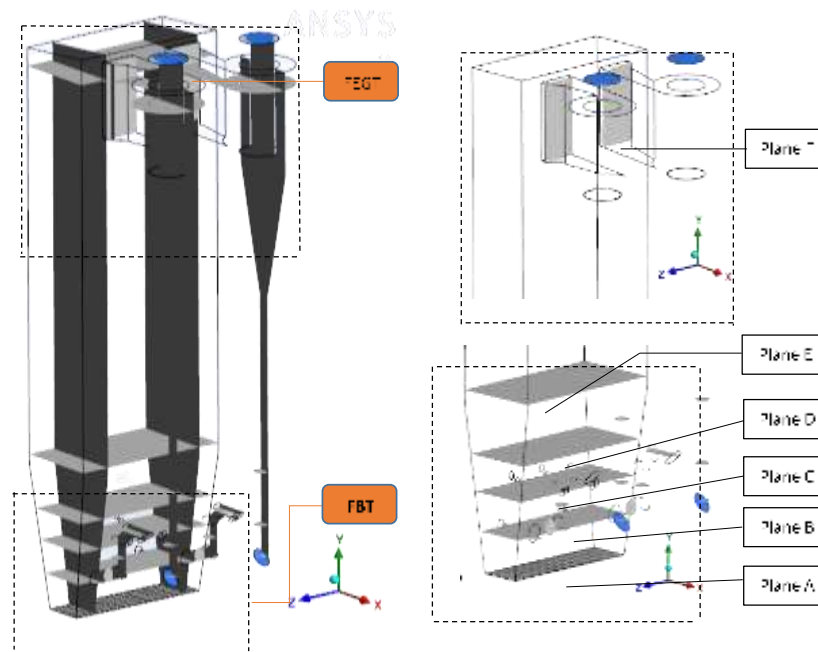

Fig. 4. Plane position in the furnace

3. Result and Discussion
3.1 Model Validation

The simulated boiler geometry is simplified to simplify computation and save costs, but the main parts are made as close to the real shape as possible. With a simpler form, it will make it easier to achieve convergence. Convergence is achieved at approximately 4000 − 7000 iterations for each variation of the simulations carried out. Furnace Bed Temperature is the area where the combustion process begins on the fluid bed. Path line checking is carried out to check the flow of fluid in the furnace. Path line checks are carried out along the furnace and starting from the primary inlet to exiting the cyclone outlet shown in Figure 5.
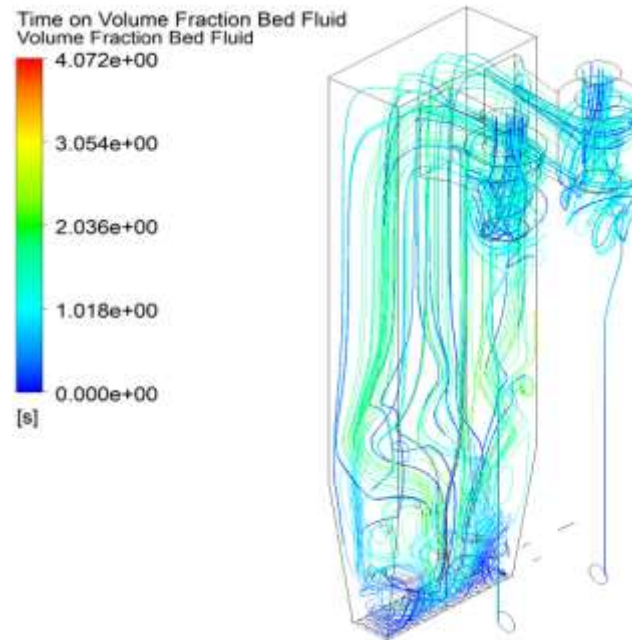
Fig. 5. Air path line volume fraction bed fluid

The path line shows the path of air flowing through the Furnace Bed Temperature and the flow occurring through the coal inlet and secondary inlet nozzles. After passing through the nozzle, it appears that the air passages fill all the furnace chambers, the movement of the air passages is also assisted by the bed fluid, which also fills the fluidized space. The air passage managed to escape through the cyclone outlet and some towards the recycle fuel device, where the component is a collection point for the remaining fly ash and bed fluid carried through the Gas Temperature Furnace Exit. The movement of the bed fluid can also be seen in Figure 6. we can see the volume fraction concentration in the area around the lower furnace, and it starts to fill the furnace space.

3.2 Simulation Data Validation
3.2.1 Data comparison of PLTU West Kalimantan simulation 0% PKS

In this simulation, the value validation from the simulation results was carried out at a point 18 cm above the Furnace Bed Temperature (position 1.3 m) and Furnace Exit Gas Temperature against the value of experimental data conducted by PLTU West Kalimantan. Data validation was carried out on the variation of mixing between coal and biomass with a variation of 0%. By the experiments carried out, the temperature contour above the Furnace Bed Temperature and Furnace Exit Gas Temperature can be seen in Figure 6 below.
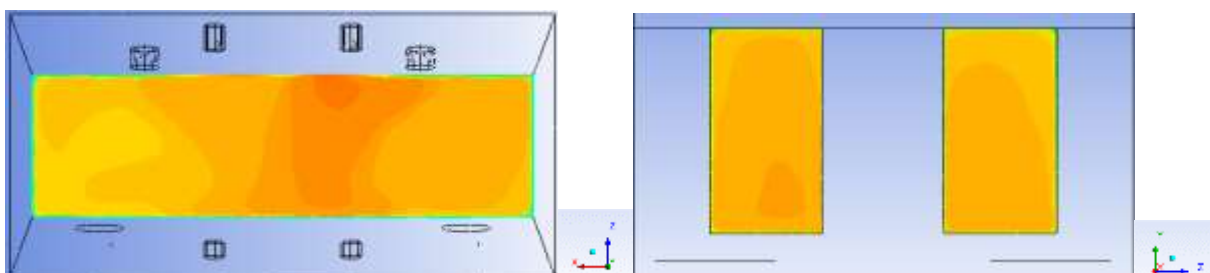

Fig. 6. Temperature contour above FBT (Furnace Bed Temperature) and FEGT (Furnace Exit Gas Temperature) 0% PKS

A comparison of the temperature values of the 0% PKS mixture carried out by the West Kalimantan PLTU to the experimental results at Furnace Bed Temperature & Furnace Exit Gas Temperature can be seen in Table 4 below.

Table 4
Data Validation of Percentage Temperature of 0% PKS Results of Simulation and Experiment Results of PLTU West Kalimantan

Measurement Position	Simulation of 0% PKS	Value (°C)	Error (%)
Furnace Bed Temperature	PLTU West Kalimantan	935.11	3.57
	Experimental Results	966.85	
Furnace Exit Gas Temperature	PLTU West Kalimantan	899.01	6.49
	Experimental Results	906.75	

3.2.2 Validation of simulation result data on research by Mahidin et al., [18]

The simulation results in this study were compared with those of Mahidin *et al.,* [18], to show that the research was close to correct. The results of the comparison can be seen in Figure 7. It can be seen that the trend in both graphs is decreasing; this is due to the increase in biomass, a significant decrease in temperature occurs. The difference in temperature values is quite large due to differences in the percentage of mixing PKS (palm kernel shell) fuel between the two studies.
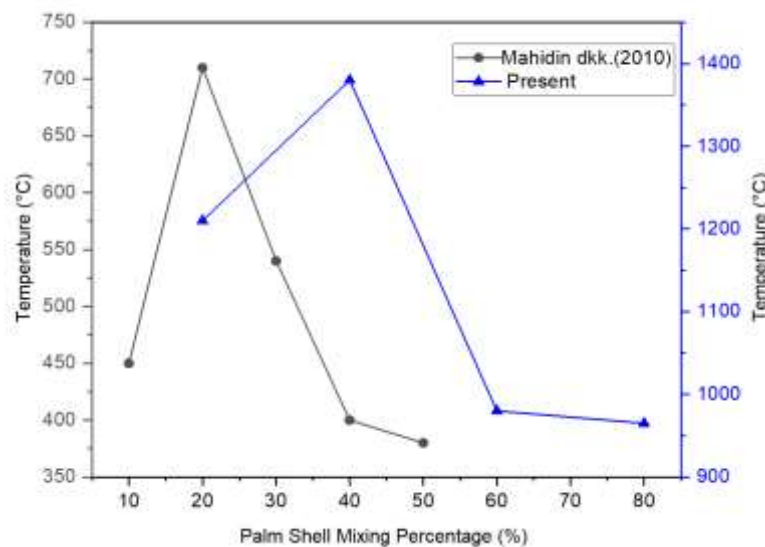
Fig. 7. Comparison of simulation results of temperature distribution with research conducted by Mahidin *et al.,* (Arifin, Amrul and Irsyad, 2021)

3.2.3 Effect of mass flow rate of sand particles on erosion rate

The simulation results of variations in the flow rate of sand particles are shown in Figure 8. From the figure, it can be seen that the erosion rate increases with the increase in the mass flow rate of the particles. This condition is caused by increasing the mass flow rate, the more particles hitting the inner wall of the pipe, thus increasing the erosion rate. In measuring the erosion rate, three measurement models are used to determine the velocity exponent. The three models are Finnie, McLaury, and Oka.
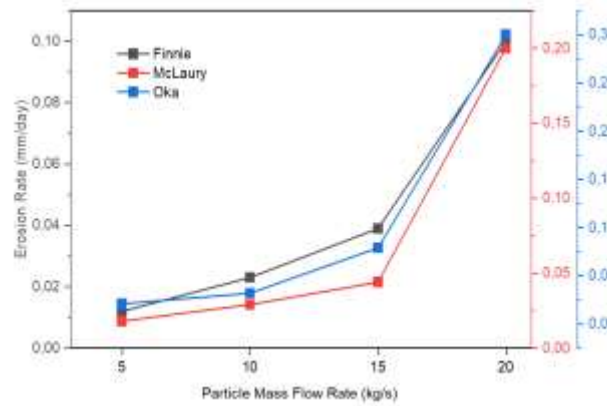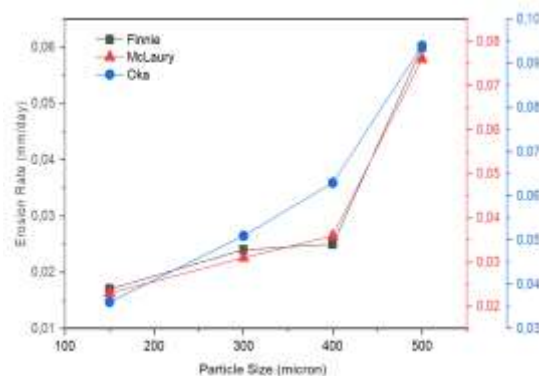
Fig. 8. Graph of effect of particle flow rate on erosion rate

Based on the measurement graph, it can be seen the erosion profile with a variation of the flow rate of 5 kg/s – 20 kg/s. At a particle flow rate of 5 kg/s, the erosion rate is the lowest, while at a particle flow rate of 20 kg/s, the erosion rate is the highest. In Ansys Fluent, the mass flow rate of the particles is used to determine the mass of the particles, which will then be included in the calculation of the erosion model. Therefore, the erosion rate with an increase in particle mass produces a linear increase, while an increase in fluid velocity results in a tendency for the erosion rate to increase exponentially according to the exponential constant used in each erosion model [15].

3.2.4 Effect of sand particle size on erosion rate

The simulation results of variations in particle size are shown in Figure 9. From the figure, it can be seen that the erosion rate increases with increasing particle size. This is by the research conducted by Tilly G., who concluded that an increase in particle size causes an increase in the erosion rate [19]. The increase in particle diameter means an increase in the mass of the particles, which at a constant speed gives greater kinetic energy of collision on the walls of the furnace.


**Fig. 9.** Graph of effect of particle size on erosion rate

Based on Figure 9, it can be seen that the erosion value of 150 µm is smaller than that of 500 µm. The larger diameter particles may tend for the particles to descend from the larger streamlined fluid. Increasing the particle diameter also means increasing the Stokes number, which is directly proportional to the square of the particle diameter, so that the tendency of the particles not to be dominated by fluid flow is greater [18].

### *3.3 Combustion Variation Analysis*

In this section of the discussion will discuss how the characteristics of combustion in each variation in the percentage of mass mixing of PKS and coal. The characteristic under study is to see the evolution of the rise and fall of temperature in the furnace. The temperature contour shown at the predetermined sampling position is in Figure 4. The simulated variation contour starts from 20%, 40%, 60%, and up to 80%. The results of taking temperature contour data can be seen from Figure 10 to Figure 13.
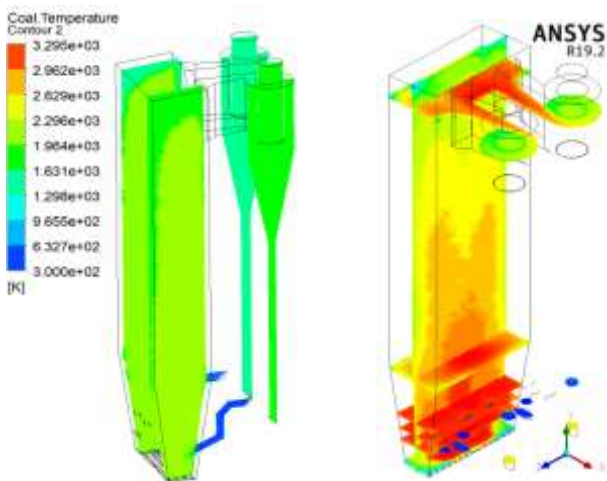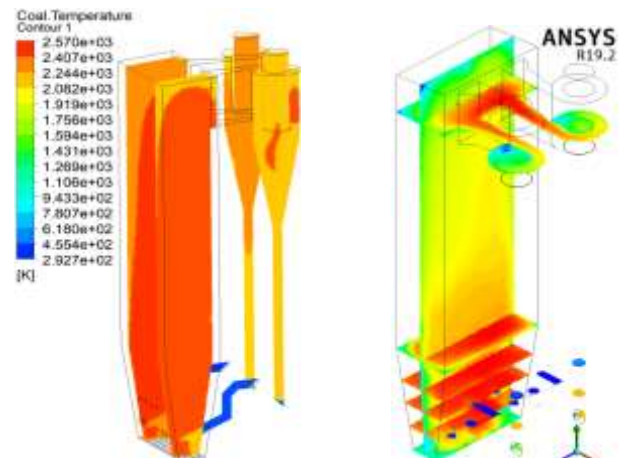

Fig. 10. Combustion temperature contour percentage of PKS mix 20%
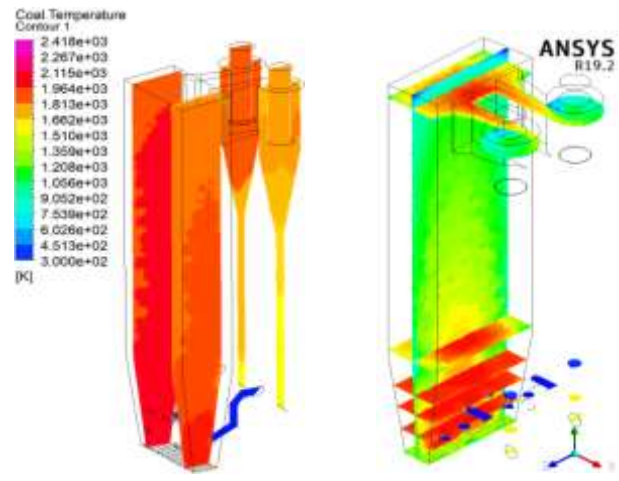
**Fig. 11.** Combustion temperature contour percentage of PKS mix 40%
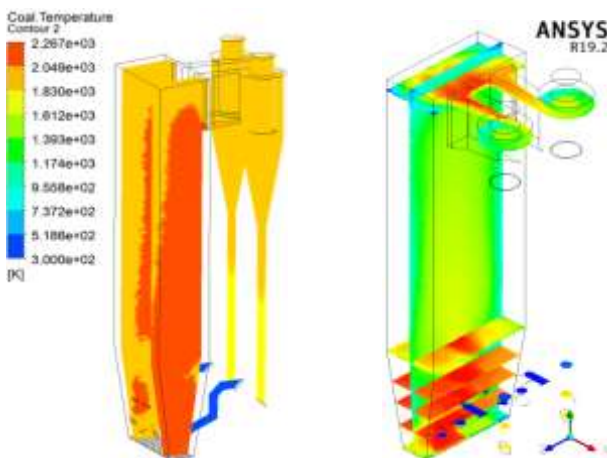
Fig. 12. Combustion temperature contour percentage of PKS mix 60%


Fig. 13. Combustion temperature contour percentage of PKS mix 80%

Based on Figure 10 to Figure 13, several analysis results can be made, namely (1) Combustion occurs at the furnace bed temperature area (2) The higher the temperature data measurement position, the more even the temperature distribution (3) The highest temperature in this simulation is the simulation of 20% mixing of palm shells, (4) The decrease in furnace temperature is caused by differences in the calorific values of coal and palm shells. The results of the contour data for the average temperature and maximum temperature in the furnace temperature bed area are shown in Figure 14, while the contour data for the average temperature and maximum temperature for the Furnace Exit Gas Temperature are shown in Figure 15.
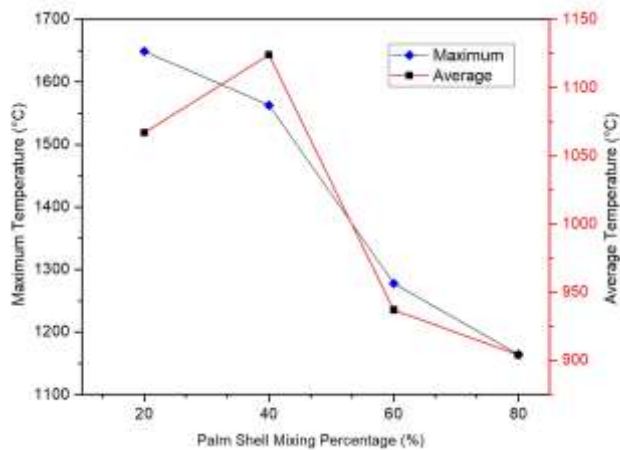
Fig. 14. Maximum and average temperature at Furnace Bed Temperature (FBT)
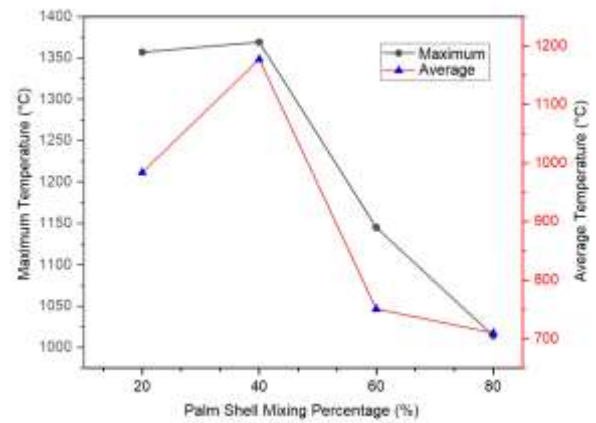

Fig. 15. Maximum and average temperature at Furnace Exit Gas Temperature (FEGT)

Based on Figure 14, it can be concluded that the average temperature distribution of variations in the simulation carried out in the Furnace Bed Temperature area decreased in temperature from 1147 ℃ to 536.21 at a variation of 40% and experienced an increase in temperature at a variation of 60%. Likewise, the Furnace Exit Gas Temperature distribution shows the same trend line where it has decreased from a 20% variation to an 80% variation. This is due to the difference in calorific value between coal and PKS (Palm Kernel Shell) fuel. Where the calorific value of coal is lower when compared to the calorific value of PKS, and it can also be caused by the proximate analysis content of different variations between coal and PKS.

As quoted in the analysis conducted by Adamczyk *et al.,*, the higher the inherent moisture value, the lower the heating value. The presence of too much water causes a decrease in the calorific value. The higher the value of volatile matter, the lower the heating value. Volatile matter contains flammable gas, it will affect the heating value. The higher the ash value, the lower the calorific value of the coal. This is due to the ash component, which can interfere with combustion. This fixed carbon is the main component of coal which is capable of generating heat in the combustion process. The higher the carbon content fixed, the calorific value of coal will increase. The higher the total sulfur value, the lower the heating value [20]. The optimal mixing value for biomass in this research simulation is the temperature value according to the Boiler Temperature Protocol (< 950).
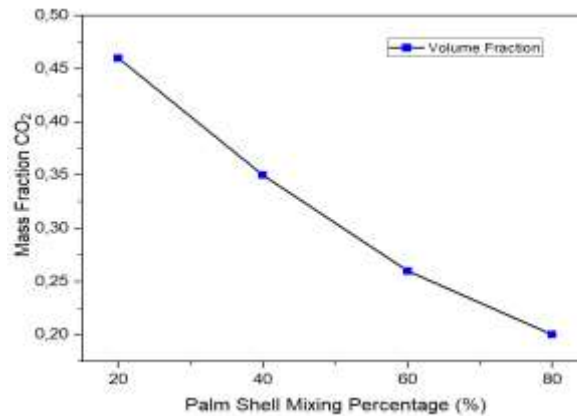
3.4 CO$_2$ Mass Fraction Analysis

One of the conditions for indication of complete combustion is when the combustion reaction where the carbon is burned out forms CO$_2$ gas. The CO$_2$ mass distribution contour data collection was carried out on Plane XY, position 4.25 m to the vertical plane. The following is the contour data for the mass fraction in the simulation variations of 20%, 40%, 60%, and 80% can be seen in Figure 16.
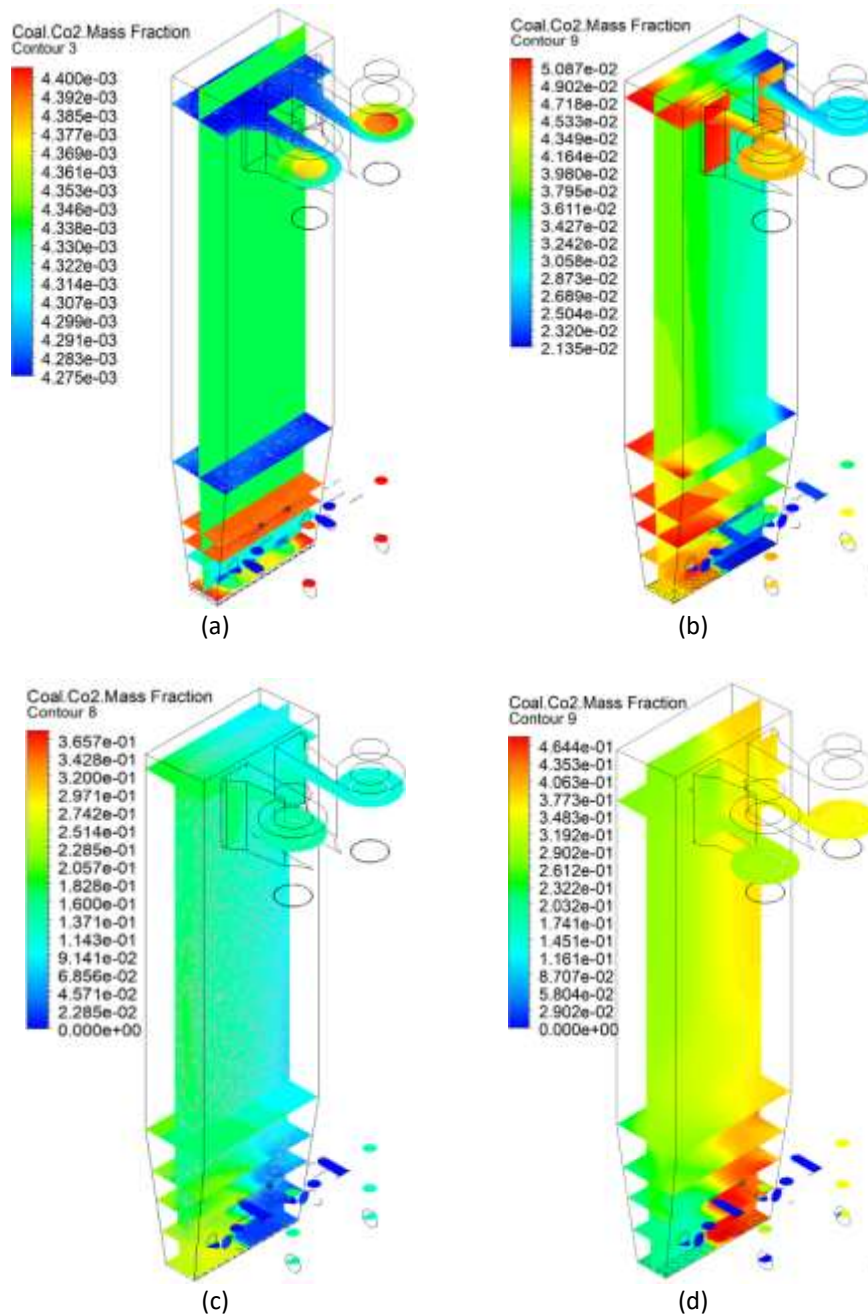
Fig. 16. CO_2 mass fraction contour (a) variation 20% (b) variation 40% (c) variation 60% (d) variation 80%

The results of the CO_2 mass fraction contour data on the XY plane in the vertical plane above show that the CO_2 fraction has decreased significantly. The increase occurred in the 20% PKS simulation variation with a CO_2 mass fraction value of 0.33976 and decreased in each simulation variation and for the 80% simulation with a CO_2 fraction value of 0.26232, as shown in Figure 17 below.

Fig. 17. CO$_2$ mass fraction contour graph simulation variation

On the graph, it can be analyzed that the fraction value decreases from a variation of 20% to a simulation of 80%. This is due to the higher PKS mass fraction resulting in lower CO$_2$ concentrations in the exhaust gas [20]. Numerically, the average CO$_2$ mass fraction in the flue gas at the combustion chamber outlet of 20%, 40%, 60%, and 80% PKS mass fraction is 0.33976, 0.27882, 027993, and 0.26232, respectively. Based on the fuel properties, coal has much higher carbon than PKS, the total amount of carbon decreases as the mass of PKS CO$_2$ fraction increases, and it also has a lower specific volume.

3.5 Fluid-bed CFD Erosion Analysis

Based on the simulations that have been carried out, the solution for the sand velocity profile distribution can be seen in Figure 18 for the flow velocity contour taken from the Bed-Fluid phase simulation. Where it shows the highest speed is in the Primary Inlet area, where sand particles are released into the furnace area at a speed of 3.2 kg/s.
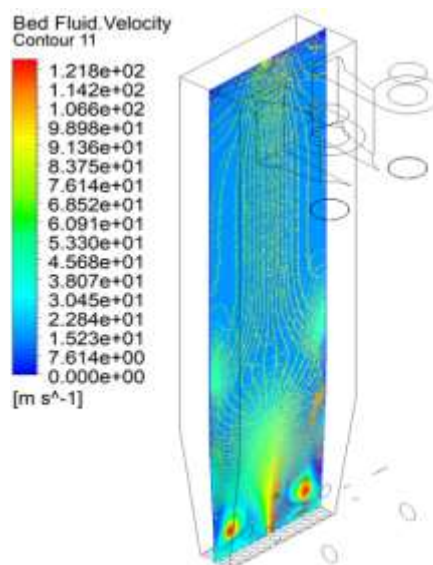
Fig. 18. Velocity profile based on velocity magnitude contours

The CFD prediction of the distribution path of sand particles shown in Figure 19 is taken from Figure 18 to determine the distribution path of the particles entering the furnace. The sand particles are expected to focus on spreading and hitting the coal inlet, secondary inlet area, where the impact will cause the sand particles to spread to the furnace walls and cause erosion on the walls [17].
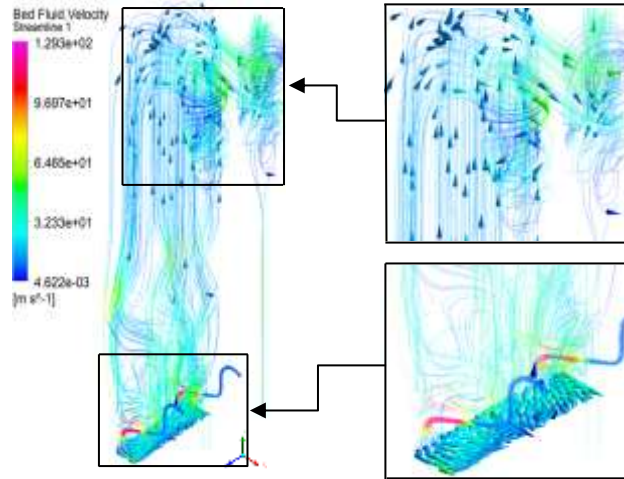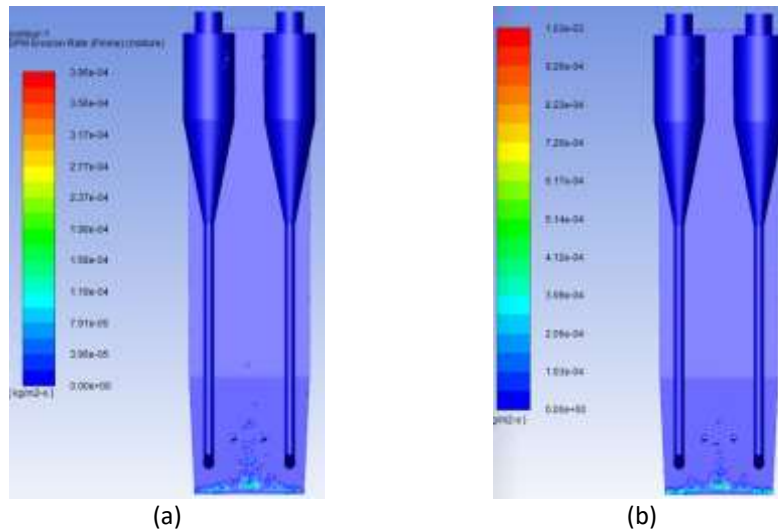

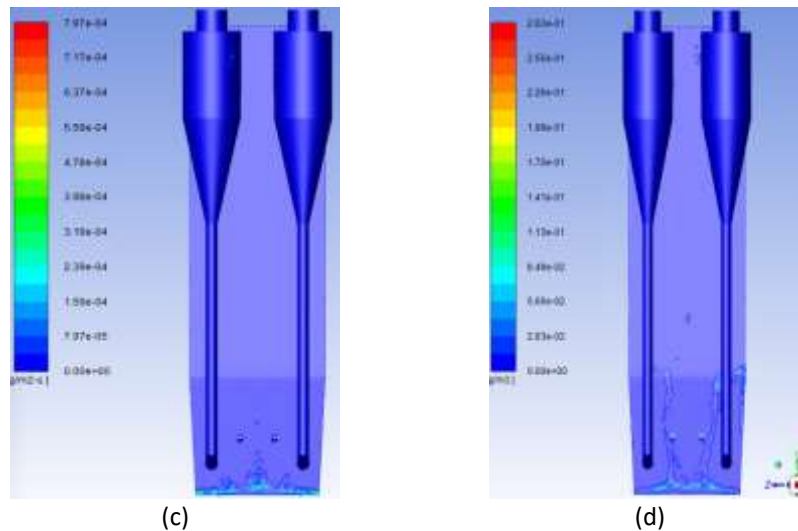**Fig. 19.** Distribution of sand particles in the furnace

Based on the velocity magnitude and the distribution of the sand particle paths, the erosion that occurs on the furnace wall during the simulation can be seen in Figure 20.

(a)　　　　　　　　　　　　　(b)

(c)   (d)

Fig. 20. Picture of the erosion rate that occurs on the furnace walls due to sand particles (a) erosion rate at 150 μm particle size (b) erosion rate at 300 μm particle size, (c) erosion rate at 400 μm particle size, (d) erosion rate at 500 μm particle size.

The prediction of the CFD erosion rate based on the simulations that have been carried out for each variation of PKS mixing can calculate the erosion rate per year. The following is the result of calculating the erosion rate of the bed fluid in Table 5 below.

Table 5
Erosion rate value data

Particle Mass Flow Rate (kg/s)	Particle Size (μm)	Sand Erosion Rate (kg/m2s)	Validation Data mm/kg	mm/kg
5	150	0.000189	0.0073	0.0369
10	300	0.000229	0.0089	0.0896
15	400	0.000796	0.0311	0.4661
20	500	0.001886	0.0737	1.4752

Based on the Erosion Rate Bed Fluid data for each simulation, the erosion rate will change as the flow of sand particles increases. The greater the flow of sand particles in each simulation, the greater the rate of erosion that occurs [16]. This is because the pressure that the orifice gets to hold back the speed of sand particles is getting bigger so that the erosion rate has a value that is directly proportional to the speed of the fluid or particles. In addition, the erosion rate has an inverse relationship with the lifetime or the age of the orifice.

4. Conclusion

The results of the geometry setup in the simulation are carried out with multiphase, namely three phases. For the properties of each Phase, part of it comes from company data and part of it comes from the fluent database. The validation stage of the simulation using geometry set up with experimental data from the West Kalimantan PLTU. The validation results of the 0% PKS mass mixing simulation at the point of measurement at FBT (furnace bed temperature) with an error value of 3.57% and at FEGT (Furnace Exit Gas Temperature) with an error value of 6.49% can be seen in Table 4. Analysis of the temperature distribution in each variation of the simulation shows that the average temperature distribution in the FBT (Furnace Bed Temperature) area increases starting from the

percentage of 20% PKS mixture with an average temperature value of 1101.8℃, then for the 40% PKS variation with a temperature value of 1120.9℃. Then from the 40% simulation, it decreased to 80% simulation. In the simulation 60% with a temperature value of 962.04℃, a variation of 80% with a temperature value of 920.03℃. Analysis of the contour distribution of the CO_2 mass fraction in Figure 16 shows that the value of the fraction decreases from the simulation of 20% - 80%. Based on Table 5, it can be seen that the greater the mass flow rate of the particles and the size of the sand particles, the greater the erosion rate that occurs on the furnace wall. The particle mass flow of 5 kg/s and a particle size of 150 μm has the lowest erosion rate, which is 0.000189. Whereas in the particle mass flow of 20 kg/s with a sand particle size of 500 μm, the erosion rate is the highest, namely 0.001886. The erosion simulation results can be used as a consideration for orifice replacement at PLTU West Kalimantan. In addition, the results of this study can be used as a reference for further research.

Acknowledgement

References

[1] Utina, Ramli. "Pemanasan global: dampak dan upaya meminimalisasinya." *Jurnal Saintek UNG* 3, no. 3 (2009): 1-11. https://doi.org/10.1016/B978-008046620-0/50035-9

[2] Ragland, Kenneth W., Kenneth M. Bryden, and Song-Charng Kong. *Combustion engineering*. Boca Raton, FL: CRC press, 2011. https://doi.org/10.2307/3102126

[3] Rozainee, M., S. P. Ngo, Arshad A. Salema, and K. G. Tan. "Computational fluid dynamics modeling of rice husk combustion in a fluidised bed combustor." *Powder Technology* 203, no. 2 (2010): 331-347. https://doi.org/10.1016/j.powtec.2010.05.026

[4] Dennis, J. S., A. N. Hayhurst, and S. A. Scott. "The combustion of large particles of char in bubbling fluidized beds: the dependence of Sherwood number and the rate of burning on particle diameter." *Combustion and Flame* 147, no. 3 (2006): 185-194. https://doi.org/10.1016/j.combustflame.2006.08.007

[5] Madhiyanon, T., A. Techaprasan, and S. Soponronnarit. "Mathematical models based on heat transfer and coupled heat and mass transfers for rapid high temperature treatment in fluidized bed: Application for grain heat disinfestation." *International journal of heat and mass transfer* 49, no. 13-14 (2006): 2277-2290. https://doi.org/10.1016/j.ijheatmasstransfer.2005.11.020

[6] Okita, Risa, Yongli Zhang, Brenton S. McLaury, and Siamack A. Shirazi. "Experimental and computational investigations to evaluate the effects of fluid viscosity and particle size on erosion damage." (2012): 061301. https://doi.org/10.1115/1.4005683

[7] Zhang, Y., E. P. Reuterfors, B. Sf McLaury, S. A. Shirazi, and E. F. Rybicki. "Comparison of computed and measured particle velocities and erosion in water and air flows." *Wear* 263, no. 1-6 (2007): 330-338. https://doi.org/10.1016/j.wear.2006.12.048

[8] Zhang, Yongli, Risa Okita, Stephen Miska, Brenton S. McLaurt, Siamack A. Shirazi, and Edmund F. Rybicki. "CFD Prediction and LDV Validation of Liquid and Particle Velocities in a Submerged Jet Impinging a Flat Surface for Different Viscosities and Particle Sizes." In *Fluids Engineering Division Summer Meeting*, vol. 43727, pp. 625-635. 2009. https://doi.org/10.1115/FEDSM2009-78333

[9] Hossain, Abu Noman. "Combustion of solid fuel in a fluidized bed combustor." Master's thesis, Ohio University, 1998.

[10] Kumar, Ravindra, and K. M. Pandey. "CFD analysis of circulating fluidized bed combustion." *Engineering Science and Technology* 2, no. 1 (2012): 163-174.

[11] Suksuwan, Wasu, Makatar Wae-hayee, and Maizirwan Mel. "The effect of single and double air inlets on swirling flow in a reactor of a fluidized bed gasifier." *Journal of Advanced Research in Fluid Mechanics and Thermal Sciences* 44, no. 1 (2018): 157-166.

[12] Liu, Hui, Ali Elkamel, Ali Lohi, and Mazda Biglari. "Computational fluid dynamics modeling of biomass gasification in circulating fluidized-bed reactor using the Eulerian–Eulerian approach." *Industrial & engineering chemistry research* 52, no. 51 (2013): 18162-18174. https://doi.org/10.1021/ie4024148

[13] Versteeg, Henk Kaarle. *An introduction to computational fluid dynamics the finite volume method, 2/E*. Pearson Education India, 2007. https://doi.org/10.1109/mcc.1998.736434

[14] Marshall, Elizabeth Marden, and André Bakker. "Computational fluid mixing." *Handbook of industrial mixing: science and practice* (2003): 257-343. https://doi.org/10.1002/0471451452.ch5

[15] Finne, I. "Erosion of surfaces." *Wear* 3, no. 2 (1960): 87-103. https://doi.org/10.1016/0043-1648(60)90055-7

[16] McLaury, Brenton S., Siamack A. Shirazi, John R. Shadley, and Edmund F. Rybicki. "Modeling erosion in chokes." *ASME-Publications-Fed* 236 (1996): 773-782.

[17] Oka, Y. I., and T. Yoshida. "Practical estimation of erosion damage caused by solid particle impact: Part 2: Mechanical properties of materials directly associated with erosion damage." *Wear* 259, no. 1-6 (2005): 102-109. https://doi.org/10.1016/j.wear.2005.01.040

[18] Arifin, Zaenal, Amrul Amrul, and Muhammad Irsyad. "Simulasi co-combustion batubara dan biomassa tandan kosong kelapa sawit tertorefaksi (torrefied biomass)." *Turbo: Jurnal Program Studi Teknik Mesin* 10, no. 1 (2021): 53-60. https://doi.org/10.24127/trb.v10i1.1468

[19] Tilly, G. P. "A two stage mechanism of ductile erosion." *Wear* 23, no. 1 (1973): 87-96. https://doi.org/10.1016/0043-1648(73)90044-6

[20] Adamczyk, Wojciech P. "Application of the numerical techniques for modelling fluidization process within industrial scale boilers." *Archives of Computational Methods in Engineering* 24, no. 4 (2017): 669-702. https://doi.org/10.1007/s11831-016-9186-z